EUROPEAN MECHANICAL SCIENCE

Research Article

e-ISSN: 2587-1110

The hole-bearing behavior of laminated composites under double-shear tension and pin-crush loading

Kenan Cinar[1*]

[1] Tekirdağ Namık Kemal University, Çorlu Faculty of Engineering, Department of Mechanical Engineering, Çorlu, Türkiye

Abstract: The bearing performance of holes in laminated composite materials is a critical research area due to their increasing use in aerospace and structural applications. This study investigates the mechanical behavior of hole-bearing in laminated composites, focusing on failure mechanisms, load distribution, and the influence of laminate stacking sequences on bearing performance. Finite element analysis (FEA) and experimental testing were used to examine stress concentration around the hole. Additionally, the digital image correlation (DIC) method was employed to monitor the strain field in the pin-bearing zone during the pin-crush test. Results indicate that fiber orientation significantly affects load-bearing capacity, with notable differences between unidirectional (UD) and cross-ply (XP) laminates. A comparison between double-shear tensile loading and pin crush loading for XP and UD samples with 16 plies reveals distinct differences in load-bearing capacity and failure behavior. In the tensile test, XP-16 samples exhibited a gradual increase in load, reaching a peak of approximately 14 kN, followed by a gradual decline. Conversely, the pin-crush test resulted in a lower peak load of 9 kN and exhibited more catastrophic failure, characterized by a sudden drop in load. In contrast, UD samples displayed similar behavior under both loading conditions, with differences observed only at peak load values.

Keywords: fiber reinforced composites; hole bearing; finite element analysis (FEA); Hashin's failure theory.

1. Introduction

Laminated composite materials are widely used in aerospace, automotive, and marine applications due to their superior strength-to-weight ratio, tailored mechanical properties, and excellent fatigue performance. One critical design aspect for bolted or riveted joint applications in these composites is their bearing behavior, which governs the load transfer efficiency and overall joint performance. The performance of hole bearings in laminated composites differs significantly from that in traditional metallic materials, primarily due to the anisotropic nature of composites. The mechanical behavior of laminated composites is influenced by several factors, including the fiber orientation, ply stacking sequence, laminate thickness, and the geometry of the hole. These factors lead to complex stress distributions, which can significantly affect the bearing strength and the potential for damage initiation around the hole, such as delamination, matrix cracking, and fiber pull-out. Over the past decades, significant research has been dedicated to understanding and predicting the bearing response of laminated composites, both experimentally and through finite element modeling (FEM).

Experimental investigations have extensively analyzed the bearing response of laminated composites, highlighting the role of material properties, lay-up configurations, and geometrical parameters. Early studies demonstrated the sensitivity of bearing strength to fiber orientation, resin properties, and ply thickness [1-7]. For instance, Furtado et al. [1] found that increasing ply thickness leads to more complex failure regions, with extensive delamination, matrix cracking, and fiber splitting near the hole. Higher ply thickness significantly reduces both the bearing load at the first load drop and the ultimate bearing load. Thin-ply laminates outperformed baseline laminates, with 21% higher initiation and 10% higher maximum bearing stresses, while thick-ply laminates showed reduced strengths. The superior performance of thin-ply laminates is attributed to their enhanced damage suppression, higher in-situ strengths, and better ply constraining. Experimental findings [5, 6] emphasized that bolted joints with ap-

*Corresponding author:
Email: kcinar@nku.edu.tr

Cite this article as:

Cinar, K. (2025). The hole-bearing behavior of laminated composites under double-shear tension and pin-crush loading. *European Mechanical Science*, 9(2): 139-154. https://doi.org/10.26701/ems.1643484

History dates:

Received: 20.02.2025, ***Revision Request***: 29.04.2025, ***Last Revision Received***: 05.05.2025, ***Accepted***: 08.05.2025

propriate preload enhance bearing strength by minimizing local damage and delamination. Lim et al. [6] examined the fatigue behavior of bolted joints in $[\pm\theta/0_8]_s$ laminates, considering ply angle θ and bolt clamping pressure, and compared results with $[0_2/\pm45_3/90_2]_s$ laminates optimized for static loading. They found that laminates whose major plies are stacked in the axial direction are suitable for bolted joints under fatigue loads if appropriate clamping pressure is applied. Khashaba et al. [7] highlighted that ±45° layers enhance bearing load and displacement, while 90° layers resist pin displacement and increase energy absorption through interlaminar shear, improving durability and delaying sudden failure. Additionally, 0° layers maximize ultimate load capacity and apparent bearing stiffness, contributing to structural reliability.

Understanding failure mechanisms is critical for optimizing bearing performance. Experimental observations have identified three primary failure modes: bearing, shear-out, and net-tension [4]. Bearing failure, characterized by compressive deformation around the hole, is the most desirable due to its progressive nature and higher load-carrying capacity. In contrast, shear-out and net-tension failures are brittle and catastrophic. From a geometrical perspective, net-tension failure occurs when the specimen's width is too narrow to alleviate high normal stress gradients, corresponding to a low width-to-diameter (w/d) ratio. Shear-out failure arises in laminates that have sufficient width to resist net-tension failure but lack adequate free edge distance to relieve high shear stresses along the shear-out plane, indicated by a low edge-to-diameter (e/d) ratio. In both net-tension and shear-out failure modes, the compressive stresses at the bearing plane are insufficient to cause significant fiber failure before these modes occur. Bearing failure, on the other hand, results from compressive stresses and involves matrix cracking, fiber micro-buckling, kinking, and substantial delamination [8].

Non-destructive evaluation techniques, such as X-ray computed tomography (CT) [9] and digital image correlation (DIC) [10-12], have been employed to characterize damage evolution in laminated composites under bearing loads. Broutelle et al. [10] investigated damage mechanisms in an oxide/oxide ceramic matrix composite bearing using the balanced quarter hole (BQH) test, enables direct observation of damage progression during bearing failure. Unlike standard bearing tests, which rely on post-mortem analysis potentially affected by cutting operations, their setup uses high-speed cameras for real-time monitoring and damage chronology. The setup's validity was confirmed through comparisons with standard tests. Two stacking sequences were analyzed, considering the effects of material microstructure and machining. Results revealed that matrix cracks appeared before the load drop, initiating delamination and kink bands, which ultimately led to failure.

FEM has emerged as a powerful tool for predicting the bearing behavior of laminated composites, offering insights into stress distributions and failure mechanisms. Early models employed linear elastic analyses to estimate stress concentrations around fastener holes [13, 14]. However, these models failed to capture the non-linear damage progression and material degradation observed in experiments. Advancements in FEM have incorporated progressive damage models (PDMs) to simulate the initiation and growth of matrix cracking, fiber breakage, and delamination [15-22]. Hashin's failure criteria [15, 16, 20] and cohesive zone models [17,18, 20] are widely used for damage prediction in composites. For instance, Qingyuan et al. [20] developed a 3D FEM framework integrating PDMs to predict bearing strengths and observed a strong correlation with experimental data. Further developments include multi-scale modeling approaches, which bridge the microscale (fiber-matrix interactions) and macroscale (laminate response) [19]. Shipsha and Burman [22] developed a multi-scale FEM model to study the impact of fiber misalignment on bearing strength, showing that local defects significantly reduce load capacity. Instead of explicitly modeling fiber bundles, the model used stiffness matrix rotations to account for bundle waviness, reducing computational costs. It incorporated LaRC04 failure criteria and an energy-based damage evolution model, accurately predicting damage mechanisms, stress levels, and failure progression, although kinking predictions were slightly conservative. The model effectively captured both intra- and inter-laminar progressive damage, offering a balance of simplicity and predictive accuracy. Parametric studies using FEM have explored the effects of various factors on bearing performance. For example, the effect of the washer type and initial bolt tension on bearing failure was investigated by Qingyuan et al. [20]. A comparison of the bearing failure states in composite bolted joints with different washers revealed that washers significantly expand the damage range, with larger washers having a more pronounced effect. However, washers reduce delamination damage due to their suppression of peak pressure and redistribution of pressure. Regarding initial bolt tension, joints with higher tension exhibited more severe matrix and delamination damage, as the increased tension delays the reduction of structural load during tensile loading. This delay allows for greater damage accumulation before failure. High initial bolt tension improves bearing strength, delays failure onset, and enhances the load-carrying capacity of joints. Recent studies have focused on the enhancement of bearing strengths using fiber continuity around holes [23, 24].

This study explores the mechanical behavior of hole-bearing laminated composites, emphasizing failure mechanisms, load distribution, and the impact of laminate stacking sequence on bearing performance under double-shear tensile loading and pin-crush loading. A combined approach of finite element analysis (FEA) and experimental testing is employed to investigate stress concentration around the hole. The Hashin failure theory is utilized in the FEA simulations to model damage mechanisms accurately. Additionally,

 https://doi.org/10.26701/ems.1643484

the digital image correlation (DIC) method is applied to monitor the strain field in the pin-bearing zone during the pin-crush test, providing detailed insights into the deformation and failure processes.

2. Experimental and numerical procedures

2.1. Materials and manufacturing of the samples

The composite samples used in this study were fabricated using AS4/8552 unidirectional prepreg material, a high-performance carbon fiber reinforced epoxy system commonly used in aerospace and structural applications. The AS4 fibers, made of carbon, have a tensile strength of approximately 4433 MPa and a modulus of elasticity of 231 GPa. The matrix is made of the 8552 epoxy resin, known for its excellent mechanical properties and resistance to thermal degradation. The composite laminates were manufactured using the prepreg lay-up technique, where the AS4/8552 prepreg sheets, which are pre-impregnated with epoxy resin, were cut to the required dimensions for the stacking sequences.

The laminates were designed with various stacking sequences to study the effect of fiber orientation and ply number on the bearing behavior. The stacking sequences used in this study include: $[0]_{16}$, $[0/90]_{2S}$, and $[0/90]_{4S}$, where the notation indicates the number of plies and fiber orientation. Specifically, $[0]_{16}$ represent unidirectional laminates with 16 plies, respectively, all oriented at 0° to the laminate plane. The $[0/90]_{2S}$, and $[0/90]_{4S}$ sequences represent cross-ply laminates, with fibers oriented at 0° and 90° to the laminate plane in varying numbers of plies. The samples manufactured are given in ▶**Table 1**.

Table 1. The samples manufactured, their sizes and stacking sequences (*i*=1,2,3).

Bearing test	Stacking sequences	Thickness (mm)	Width (mm)	Length (mm)
XP-8-S*i*	$[0/90]_{2s}$	1.5±0.05	36±0.1	100±0.1
XP-16- S*i*	$[0/90]_{4s}$	3±0.05	36±0.1	100±0.1
UD-16- S*i*	$[0]_{16}$	3±0.05	36±0.1	100±0.1
Pin-crush test				
XP-16- S*i*	$[0/90]_{4s}$	3±0.05	25±0.1	100±0.1
UD-16- S*i*	$[0]_{16}$	3±0.05	25±0.1	100±0.1

The lay-up process involved carefully placing each prepreg ply on a mold to maintain fiber orientation and ensure uniform resin distribution. The prepreg sheets were layered in the desired stacking sequence, and each layer was lightly rolled to eliminate any air pockets and improve fiber-to-matrix bonding. Once the lay-up was completed, the laminate was cured in an autoclave at 120 °C for 30 minutes and followed by 180 °C for 2 hours under 7 bar pressure to ensure full resin polymerization and optimal fiber-matrix bonding. After curing, the laminates were trimmed into 100 mm × 36 mm (25 mm for pin-crush test) specimens and 6 mm diameter hole was drilled in the specified region (18 mm from the edge of the sample), as stated in the ASTM D5961. The drilling process was done carefully to prevent damage to the fibers or matrix and minimize stress concentrations around the hole. The holes were drilled using an unused TiAlN coated carbide drill bit with a 118-degree point angle, operated at a rotational speed of ~1500 rpm and a feed speed of ~100 mm/min. Visual inspection of the drilled holes revealed no observable delamination around the hole edges, as illustrated in ▶**Figure 1b**. Therefore, quantitative measurement of delamination diameter was not performed in this study. Nevertheless, future investigations may benefit from incorporating tomography-based delamination evaluation methods to further assess hole quality and damage resistance. The edges of the specimens were grinded

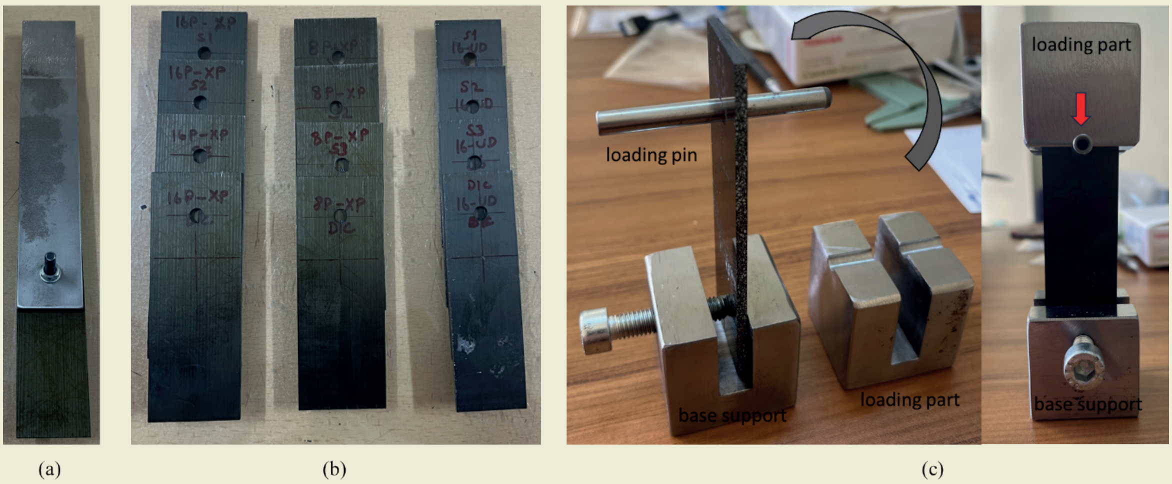

Figure 1. a) the bearing test fixture b) test samples and c) specifically designed test fixture for pin-crush test.

https://doi.org/10.26701/ems.1643484

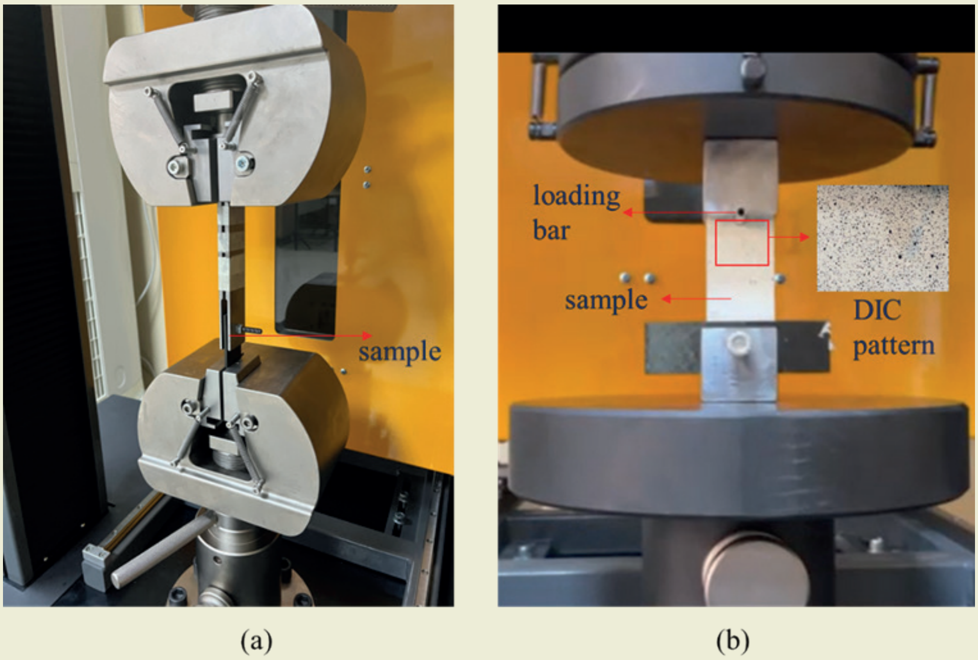

Figure. 2 a) Double-shear tensile test set-up b) strain field measurement set-up under pin-crush test

using sand papers to ensure uniform loading during testing. A special fixture as stated in the test standard (ASTM D5961) was fabricated to conduct the bearing tests, as shown in ▶**Figure 1a**. Three tests were done for each configuration. ▶**Figure 1c** presents the experimental setup used for the pin-crush test. The fixture consists of a base support with a V-groove to hold the composite specimen in place and a loading part that applies compressive force through a cylindrical pin inserted into the hole of the specimen. For Digital Image Correlation (DIC) measurements, the loading support was specifically designed with a half-hole configuration to ensure that the damage progression around the hole could be clearly captured without obstruction during the pin-crush test.

2.2. Double-shear tensile and pin-crush tests

The double-shear tensile test (bearing test) is a widely used experimental method to evaluate the performance of composite laminates under localized bearing loads, typically applied through a bolt or pin. In this study, the test was conducted using a UVE tensile test machine (200 kN) at a speed of 1 mm/min, adhering to the ASTM D5961 standard, as shown in ▶**Figure 2a**. A specially designed fixture was used to securely hold the specimens and ensure accurate load transfer, as specified in the standard. The test setup allows the investigation of the bearing strength, stiffness, and failure modes of composite materials, offering insights into their ability to withstand concentrated loads in bolted joint applications. The displacement was measured directly from the machine, capturing the mechanical response of the specimens under gradually increasing loads.

For pin-crush tests, Digital Image Correlation (DIC) was employed to capture full-field strain and displacement distributions on the specimen's surface during the test, as shown in ▶**Figure 2b**. The GOM software was used for DIC data acquisition and analysis, providing high-resolution measurements of strain evolution and damage progression. By correlating the DIC results with the load-displacement data, a detailed understanding of the material's local and global deformation behavior was achieved. This integration of bearing testing with DIC allows for a comprehensive characterization of the material's mechanical performance, highlighting critical regions of stress concentration and failure initiation in composite laminates.

2.3. Finite element analysis

▶**Figure 3** illustrates the finite element (FE) models for two different mechanical tests: the double-shear tensile test (▶**Figure 3a**) and a pin-crush test (▶**Figure 3b**). The FE mesh consists of structured and unstructured elements, with finer meshing in the regions of high stress concentration, particularly around the hole where the load is applied. The number of nodes and elements are given in ▶**Table 2**. The structured elements appear in the flat plate regions, where hexahedral meshes are used in a grid-like pattern. The unstructured elements are seen around the hole, where irregular meshing is necessary to capture stress concentrations and complex deformations. In the bearing test model in ▶**Figure 3**(a), boundary conditions were applied to ensure symmetry along the z-direction and the y-direction, restricting displacement at the edges. Thus, 8 plies were modeled. The load is applied in the x-direction with a prescribed

 https://doi.org/10.26701/ems.1643484

displacement of 4 mm at the contact region. The top region is clamped to replicate experimental constraints, and contact interactions are defined between the pin and the hole surface to capture localized deformation behavior.

In the pin-crush test model in ▶**Figure 3**(b), the boundary conditions differ to reflect a crushing scenario where the load is applied in the x-direction with a displacement of 2.5 mm. The structure is supported at the bottom, preventing rigid body motion in x-direction. The mesh refinement around the hole and the surrounding region indicates the need for accurate stress-strain predictions in highly deformed areas. The middle section of the image highlights the detailed meshing of the curved surface, which is crucial for capturing nonlinear deformations and contact effects. Both models are designed to study the material behavior under different loading conditions, providing insights into failure mechanisms such as local crushing, shear-out, or bearing failure in composite plates.

Table 2. The number of elements and nodes

Bearing analysis	Number of elements	Number of nodes
XP-8-FEM	633	1247
XP-16-FEM	2331	3319
UD-16-FEM	2331	3319
Pin-crush analysis		
XP-16-FEM	4954	5883
UD-16-FEM	4954	5883

Eight-node quadrilateral in-plane general-purpose continuum shell elements (SC8R) were used to model the lamina. To improve computational efficiency, the fixed mass scaling option in ABAQUS/Explicit [25] was activated at the start of the analysis with a scaling factor of 1000. The lamina was assumed to exhibit transversely isotropic linear elastic behavior. Hashin's damage initiation criteria were applied to predict the onset of damage, considering four distinct and uncoupled damage initiation modes, defined as follows:

$$F_f^t = \left(\frac{\sigma_{11}}{X^T}\right)^2 + \left(\frac{\tau_{12}}{S^L}\right)^2 \text{ Fiber tension } (\sigma_{11} \geq 0) \quad (1)$$

$$F_f^c = \left(\frac{\sigma_{11}}{X^C}\right)^2 \quad \text{Fiber compression} \quad (\sigma_{11} < 0) \quad (2)$$

$$F_m^t = \left(\frac{\sigma_{22}}{Y^T}\right)^2 + \left(\frac{\tau_{12}}{S^L}\right)^2 \text{ Matrix tension } (\sigma_{22} \geq 0) \quad (3)$$

$$F_m^c = \frac{1}{Y^C}\left[\left(\frac{Y^C}{2S^T}\right)^2 - 1\right](\sigma_{22}) + \frac{1}{2(S^T)^2}(\sigma_{22})^2 + \frac{1}{(S^L)^2}(\sigma_{12}^2)$$

$$\text{Matrix compression} \quad (\sigma_{22} < 0) \quad (4)$$

where, X^T and X^c are the longitudinal tensile and compressive strengths, Y^T and Y^C are the transverse tensile and compressive strengths, S^L and S^T are the longitudinal and transverse shear strength, σ_{ij} $(i = 1, 2)$ are the components of the stress tensor, α is a coefficient which determines the contribution of the shear stress to the fiber tensile criterion. The mechanical properties of a unidirectional AS4/8552 lamina are given in ▶**Table 3**. It should be noted that inter-laminar damage (delamination) was not considered in this model due to computational burden of the analysis.

Table 3. AS4/8552 material properties [26]

Property	Value	Units
Ply elastic properties		
E_1	137100	MPa
$E_2 = E_3$	8800	MPa
$G_{12} = G_{13}$	4900	MPa
G_{23}	5400	MPa
$\upsilon_{12} = \upsilon_{13}$	0.314	
υ_{23}	0.487	
Ply strength properties		
X^T	2106.4	MPa
X^C	1675.9	MPa
Y^T	74.2	MPa
Y^T	322.0	MPa
S^L	110.4	MPa
Ply fracture energies		
б$_{1+}$	125.0	kJ/m^2
б$_{1-}$	61.0	kJ/m^2
б$_{2+}$	0.3	kJ/m^2
б$_{6}$	0.87	kJ/m^2

3. Results and Discussions

3.1. Double-shear tensile test (bearing test)

The load-displacement curve in ▶**Figure 4** represents the bearing response of composite laminates under ASTM D5961 testing conditions. The laminates tested include cross-ply (XP) laminates with 8 and 16 total lamina and unidirectional laminates with 16 total laminas denoted as XP-8, XP-16 and UD-16, respectively. The average maximum bearing forces and standard deviations for the tested specimens were calculated as follows: XP-8: 5679.6 ± 294.1 N, XP-16: 14832.9 ± 517.6 N, and UD-16: 5439.6 ± 128.7 N. The black curves correspond to XP-16 samples, which exhibit higher peak loads, indicating superior bearing strength due to the increased number of a lamina. In contrast, the red curves represent XP-8 samples, which show lower peak loads, reflecting their reduced bearing capacity. Both laminate types demonstrate typical behavior under bearing loads, with an initial linear region followed

https://doi.org/10.26701/ems.1643484

by a peak and a gradual decline, indicative of material damage or failure mechanisms of matrix tensile failure, matrix and fiber crushing/fracture and delamination. The UD-16 laminates exhibit significantly lower peak loads and abrupt post-peak drops, indicative of brittle failure mechanism due to transverse matrix cracking. This comparison underscores the critical role of laminate architecture in influencing the bearing strength and failure mechanisms of composite materials, with cross-ply laminates providing enhanced performance over unidirectional ones in bearing applications.

The failure modes observed in laminated composites under a bearing test can vary depending on the laminate stacking sequence and loading conditions. Net-tension failure occurs when the specimen fractures across

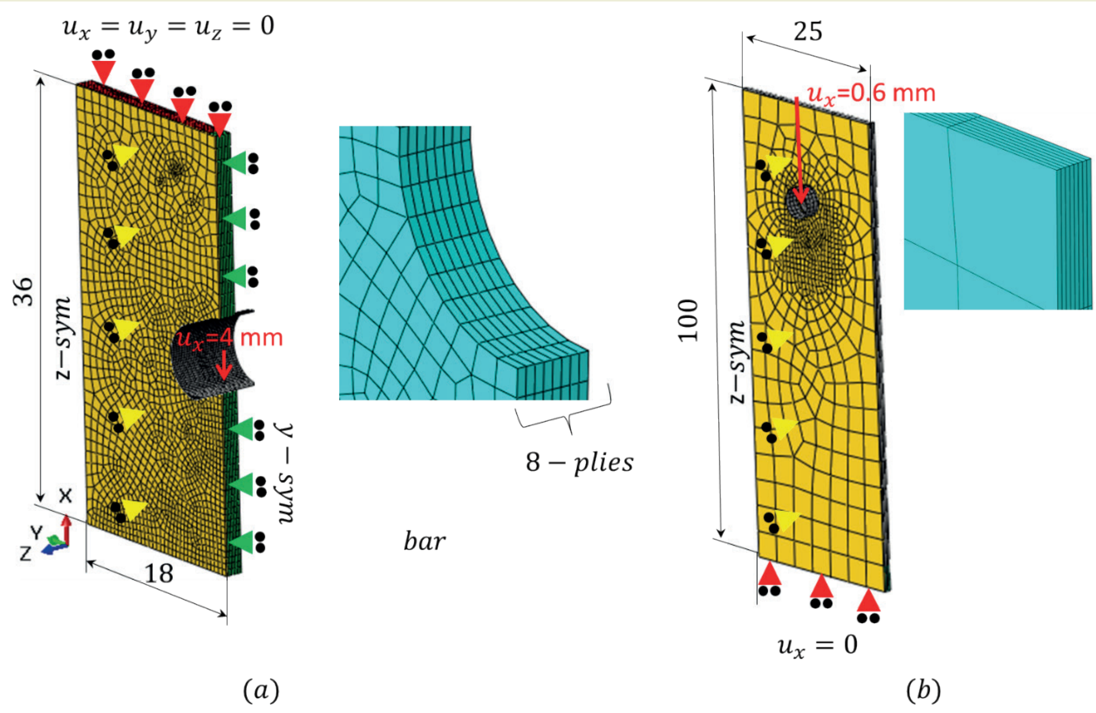

Figure 3. Finite element mesh, loading and boundary conditions a) bearing test model, b) pin-crush test model

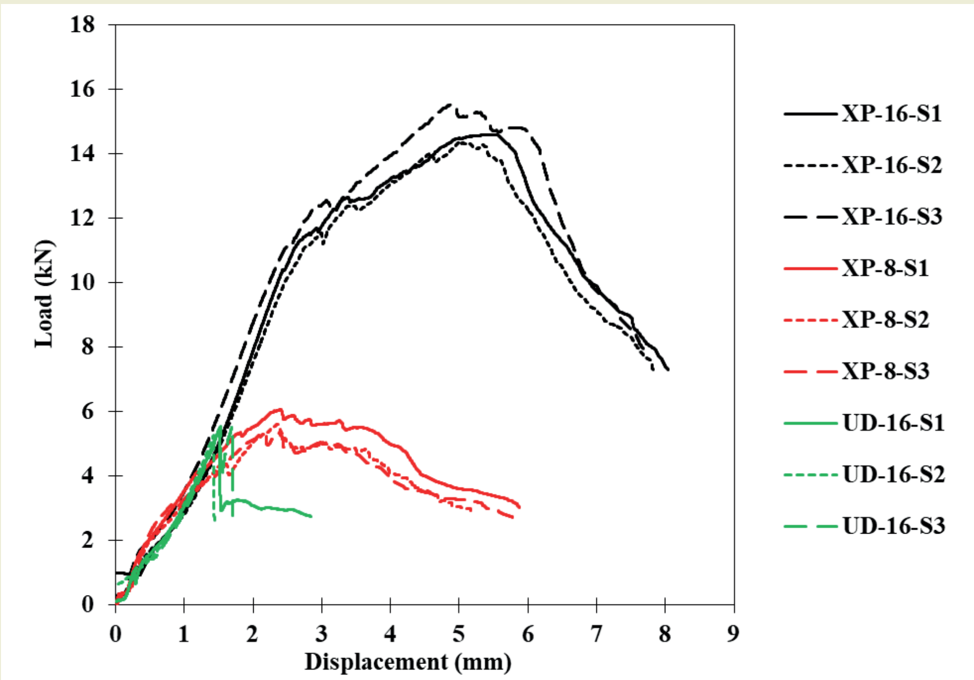

Figure 4. Load-displacement response of bearing tests for XP and UD samples with 8 and 16 plies.

its width due to excessive tensile stresses, leading to brittle failure, which is often seen in laminates with lower bearing strength [4, 8]. This failure mode was occurred in UD laminates, as shown in ▶Figure 5c. In many cases, mixed failure modes are observed, where a combination of bearing, net-tension, and shear-out failure occurs depending on the laminate stacking and test conditions. Bearing failure is characterized by progressive damage around the hole due to high localized stresses, often occurring in thicker laminates like 8-XP and 16-XP as shown in ▶Figure 5 a and 5b. The cross-ply specimens in this study exhibit signs of shear-out and bearing failure, indicating a complex interaction of stress distributions around the hole [4, 8].

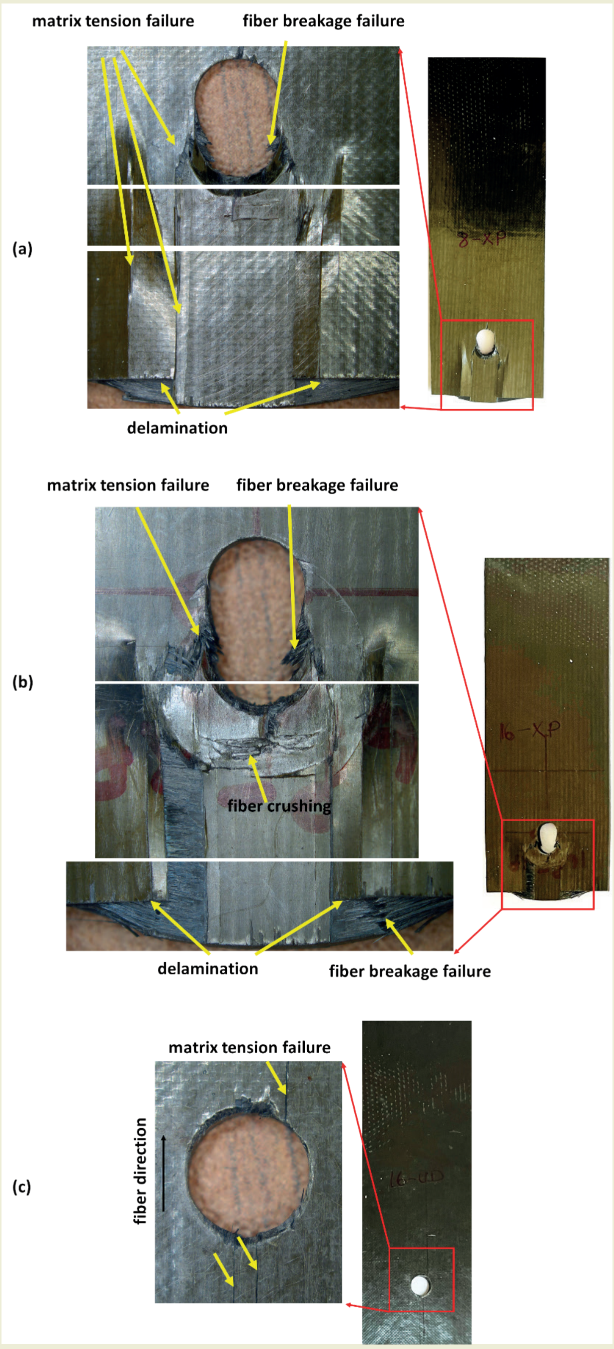

Figure 5. Failure of samples under bearing test a) 8-XP, b) 16-XP, and c) UD-16

3.2. Pin-crush tests

The pin-crush loading results for XP and UD samples with 16 plies in ▶Figure 6 show distinct differences in load-bearing capacity and failure behavior. The XP-16 reaches a higher peak load compared to the UD-16. The average maximum pin-crush forces and standard deviations for the tested specimens were calculated as follows: XP-16: 9227.5 ± 803.3 N, and UD-16: 6629.4 ± 320.3 N. Additionally, the XP sample exhibits a more gradual decline after reaching peak load, maintaining a significant load-carrying capacity (~5000 N) over a larger displacement range (~1–5 mm). This suggests a more progressive failure mechanism, likely due to enhanced load redistribution in the XP laminate. In contrast, the UD sample experiences a sharp load drop immediately after peak load, with rapid degradation beyond 1.5 mm displacement. This indicates a more brittle failure mode, where damage accumulates quickly, leading to catastrophic failure with minimal residual load-bearing capacity. Overall, the XP sample outperforms the UD sample in terms of both peak load and post-peak load retention, making it more resistant to crushing-induced damage. The improved performance of the XP laminate could be attributed to its stacking sequence, which likely enhances its resistance to through-thickness shear and progressive damage mechanisms.

This Digital Image Correlation (DIC) image in ▶Figure 7 presents the strain distribution (ε_y) in the laminated composite specimen of 16-XP undergoing the pin-crush test. The sequence of images from left to right and top to bottom suggests a progressive loading scenario, where strain concentration around the hole increases with load application. Initially, the specimen shows a uniform strain distribution with minimal localized deformation. As the load increases, strain accumulation becomes evident around the contact region between the hole and the pin, primarily in the upper part, where compressive forces are dominant. The color scale indicates that strain values transition from low (red) to high deformation (blue), with negative strain representing compression. In the intermediate stages, strain localization spreads radially from the hole, with higher deformation at the upper contact edge. The bottom edge of the hole remains relatively less affected initially, but as loading progresses, shear bands and deformation extend downward, indicating material yielding and potential bearing failure initiation. In the final images, significant localized damage appears below the hole, with clear signs of fiber-matrix separation or delamination, particularly in the lower part, suggesting shear-out failure progression. The highest strain zones (blue regions) indicate areas susceptible to crack initiation and failure propagation.

The sequence of images in ▶Figure 8 illustrates the evolution of transverse strain (ε_x) over time during a pin crushing test on a unidirectional (UD-16) laminate.

 https://doi.org/10.26701/ems.1643484

Initially, the strain distribution is relatively uniform across the specimen, with minimal localized deformation. As the test progresses, strain concentration develops directly beneath the pin, forming a vertical band of increasing tensile strain, as shown by the transition from green to yellow and red. This strain localization suggests the onset of matrix damage along the loading path. In the later stages, a significant crack propagates downward, characterized by high tensile strain (red regions) along the failure path. The final image reveals a fully developed fracture matrix crack. The test results highlight the brittle nature of the unidirectional

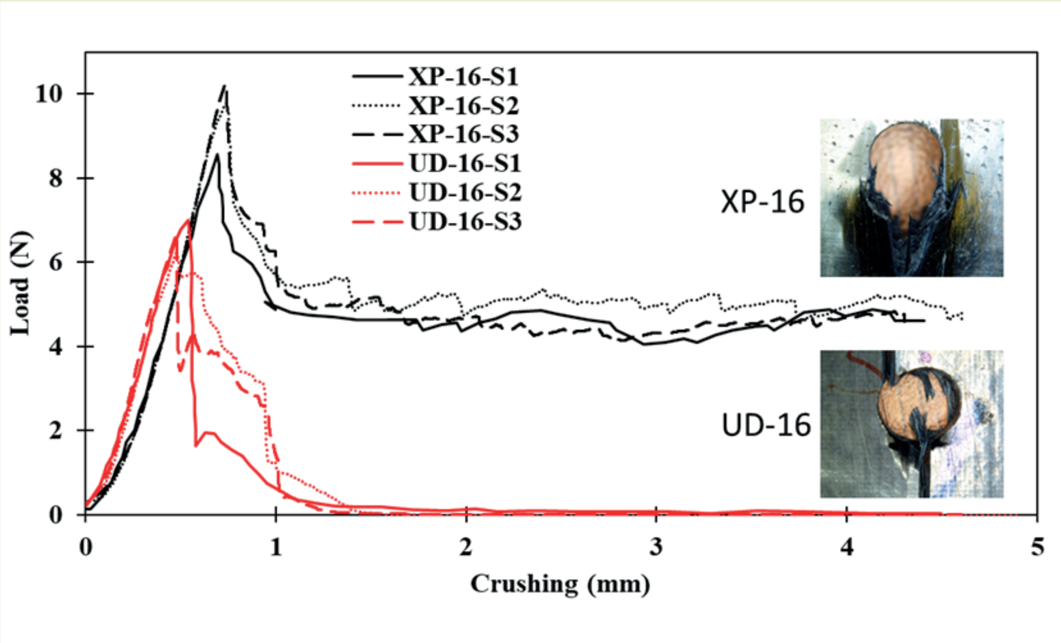

Figure 6. Load-crushing response of under specifically designed fixture for UD and XP samples of 16 plies.

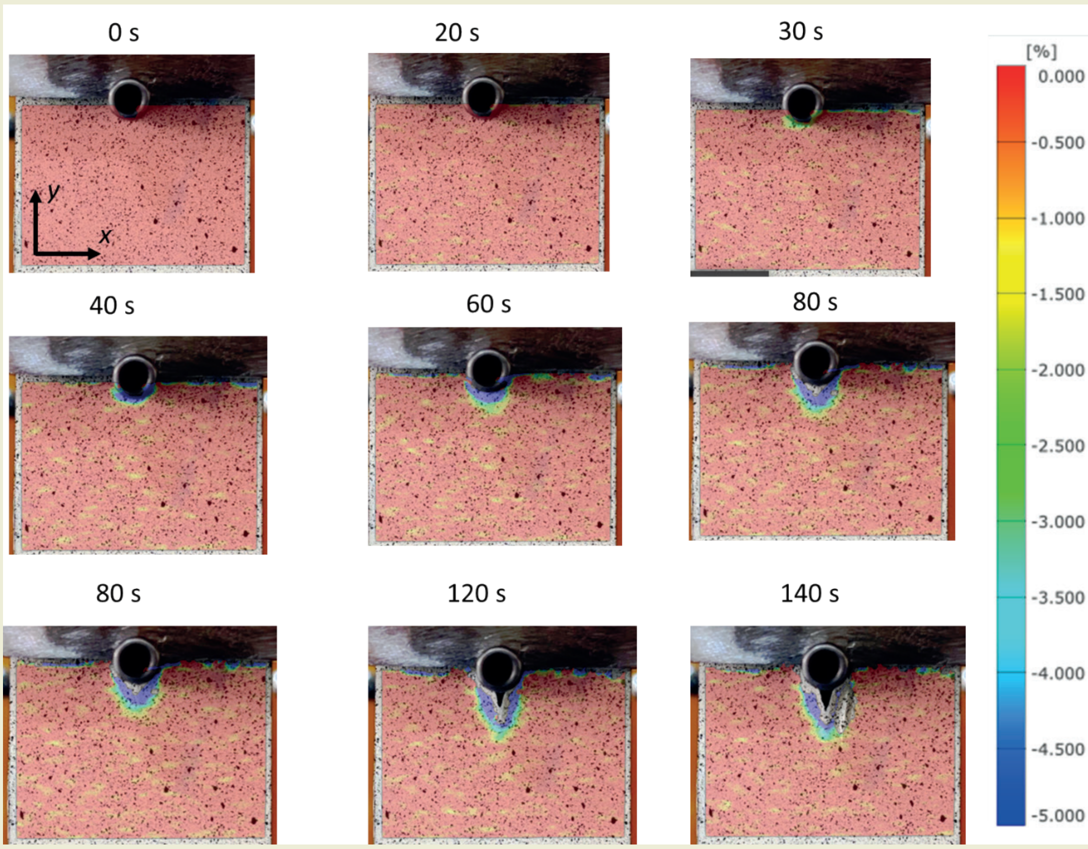

Figure 7. Change in (ε_y) with time under pin-crush test for XP-16 sample.

 https://doi.org/10.26701/ems.1643484

composite under pin crushing, where failure occurs through crack initiation at the contact point, followed by rapid crack propagation along the fiber direction. The strain distribution suggests that load transfer is primarily concentrated along the vertical axis, leading to localized damage and eventual material failure.

This sequence of images in ▶**Figure 9** illustrates the evolution of vertical strain (ε_y) over time during a pin crushing test on a unidirectional (UD-16) laminate. As the test progresses, localized strain concentration develops around the pin contact area, shown by the transition from red to green and blue regions. These areas indicate increasing compressive strain directly beneath the pin and slight tensile effects near the edges. In the later stages, strain localization intensifies along the failure path, forming a vertical crack propagating downward. The results highlight that the UD laminate primarily experiences compressive loading along the vertical axis, with failure initiating at the contact point and progressing due to local crushing and splitting. Unlike the horizontal strain (ε_x) , which exhibited more tensile behavior in the crack path, the vertical strain field remains mostly compressive, supporting the observation that failure is dominated by localized crushing and transverse matrix cracking.

3.3. Finite element analysis

To ensure the reliability of the finite element model, a mesh convergence analysis was conducted by varying the global mesh size (GMS) around the hole region. Three mesh densities were considered: GMS = 2 mm, 1 mm, and 0.5 mm, as illustrated in the inset of ▶**Figure 10**. The corresponding load-displacement curves show that as the mesh was refined, the numerical results became more stable and converged. Specifically, the model with GMS = 0.5 mm showed only slight variation in peak load compared to the 1 mm mesh, indicating that the solution had sufficiently converged. Based on this analysis, GMS = 1 mm was selected for further simulations, providing a good balance between computational accuracy and efficiency.

Figure 11 shows the load-displacement curve from the double-shear tensile test which illustrates the mechanical response of UD-16 samples, comparing experimental result with finite element method (FEM) prediction. Both curves exhibit an initial linear increase, followed by a peak and subsequent softening. The FEM prediction (UD-16-FEM) closely follow the experimental trends (dotted lines), indicating that the finite element model effectively captures the material response. However, some deviations are noticeable, particularly in the post-peak region, which could be attributed to factors such as material property variability, damage evolution modeling, or experimental uncertainties. The brittle nature of unidirectional laminates under bearing loading may cause these fluctuations, and the FEM model appears to slightly underestimate the peak load, failing to capture premature damage initiation in the real test specimens. Failure progression can also be seen in

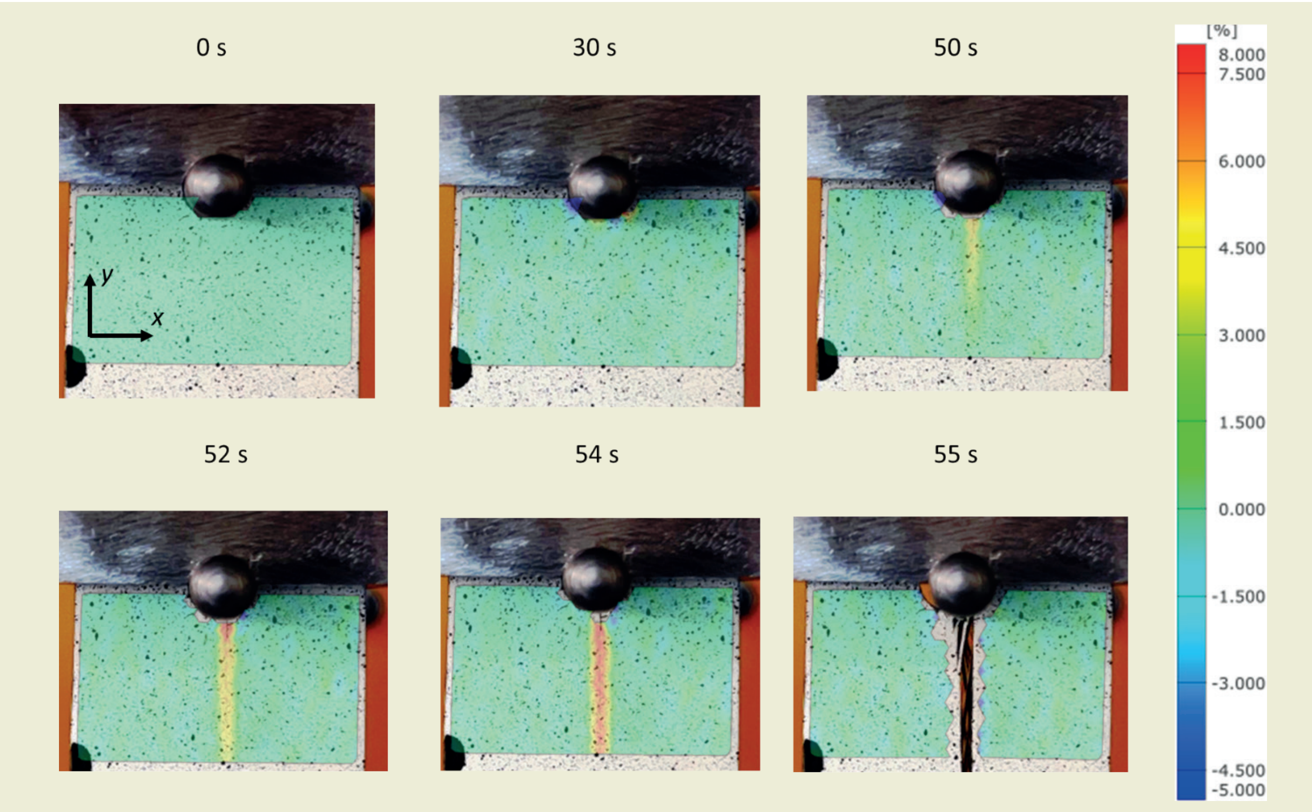

Figure 8. Change in (ε_x) with time under pin-crush test for UD-16 sample.

▶Figure 11. Hashin's matrix tensile failure index with displacement and load was represented. The progression of matrix tensile failure initiated beneath the bolt shaft region and propagated downward.

▶Figure 12 presents the results of a bearing test for the XP-8 specimen, including both experimental (XP-8-S2) and finite element model (XP-8-FEM) curves. The load-displacement graph shows that the FEM simulation closely follows the experimental trend, capturing the key load peaks and progressive failure behavior. However, some discrepancies exist, particularly in the post-peak region, where the experimental curve exhibits a more gradual decline, whereas the FEM model

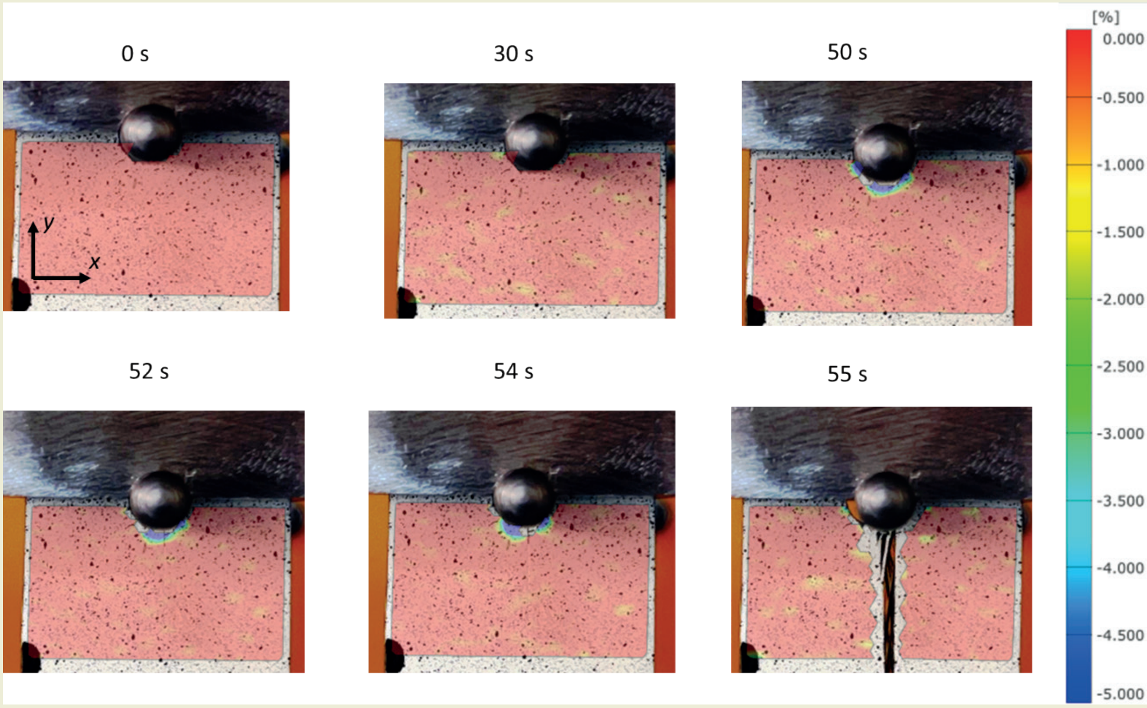

Figure 9. Change in (ε_y) with time under pin-crush test for UD-16 sample.

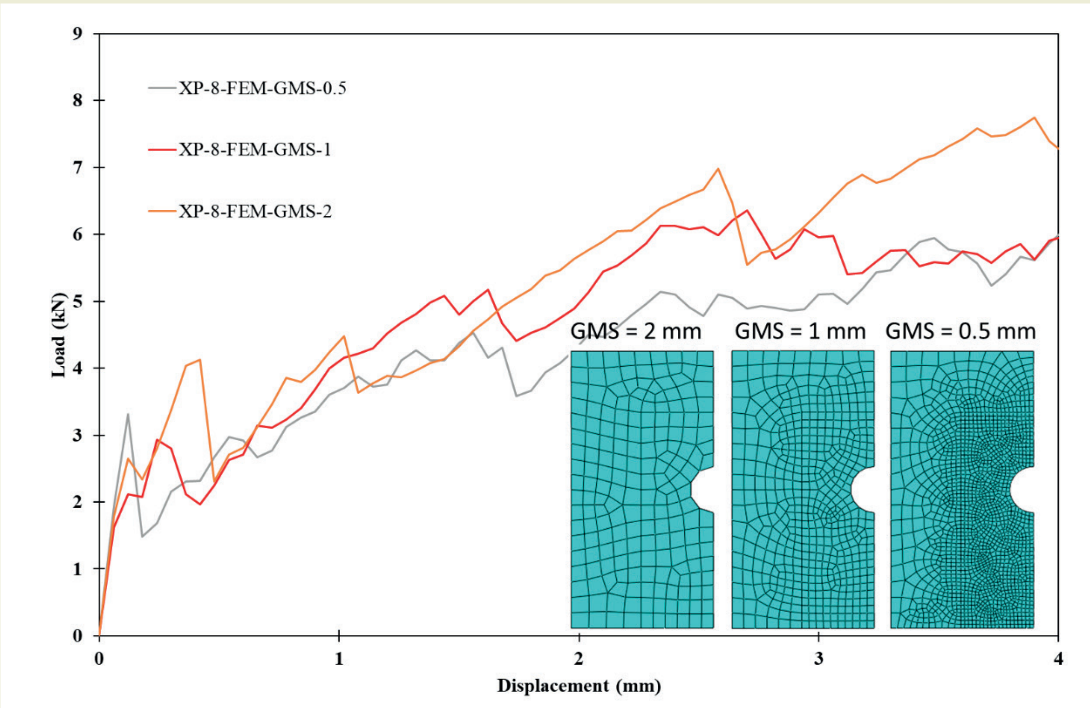

Figure 10. Mesh convergence analysis for the XP-8 specimen showing the effect of global mesh size (GMS = 2 mm, 1 mm, and 0.5 mm) on the load–displacement response.

maintains higher load levels before dropping. The peak load values are relatively close, with the FEM predicting a slightly higher failure load compared to the experiment. The Hashin failure modes in the image provide a detailed progression of damage during the bearing test. Initially, matrix tension failure occurs around the notch and spreads along the loading path as the displacement increases, indicating the onset of damage due to transverse tensile stresses. At higher load levels, matrix compression failure becomes prominent, particularly in regions experiencing compressive stresses, leading to material crushing. As the load continues to increase, fiber tension failure becomes more evident, especially in areas subject to axial stretching along the fiber direction. In the final stages, fiber tension failure becomes widespread, contributing to the reduction in load-bearing capacity. Additionally, fiber compression failure is observed near the notch where localized compressive stresses cause fiber kinking and instability. Overall, the FEM model effectively captures the initiation and evolution of these failure modes, with matrix failures occurring first, followed by fiber failures as the load increases. The FEM results correlate well with the experimental observations, but slight discrepancies in failure evolution suggest room for further refinement in the material modeling, particularly in the representation of damage propagation and softening behavior.

▶Figure 13 presents the results of a bearing test for the XP-16 specimen, including both experimental (XP-16-S1) and finite element model (XP-16-FEM) curves. The load-displacement curves demonstrate a strong correlation between the experimental and simulated results, validating the accuracy of the FEM model in predicting the material's response under double-shear tensile test. Both curves exhibited an initial linear elastic region, followed by a non-linear phase indicative of progressive damage, culminating in a load drop signifying failure. The load-displacement curve at the top illustrates a strong correlation between the two, with numbered points corresponding to specific stages of damage. Below, the image is segmented into four rows representing different Hashin failure modes: matrix tension, matrix compression, fiber tension, and fiber compression. Each column, numbered 1 through 10, corresponds to a specific displacement and load value, showing the evolution of damage over time. Initially, matrix tension damage is observed, followed by matrix compression, then fiber tension, and finally fiber compression, indicating a sequential progression of failure mechanisms. The contour plots within each segment visually represent the failure index distribution, with color gradients indicating the severity of damage for each mode. The numerical values below each column specify the displacement in millimeters and the corresponding load values, providing a quantitative measure of the material's response. It is important to note that the number of frames shown for each failure mode in **▶Figures 12 and 13** differs between specimens. For the XP-8 specimen (**▶Figure 12**), seven critical points were selected along the load-displacement curve based on noticeable changes in slope or load drops that indicate key stages in the damage evolution. In contrast, ten such points were identified for the XP-16 specimen (**▶Figure**

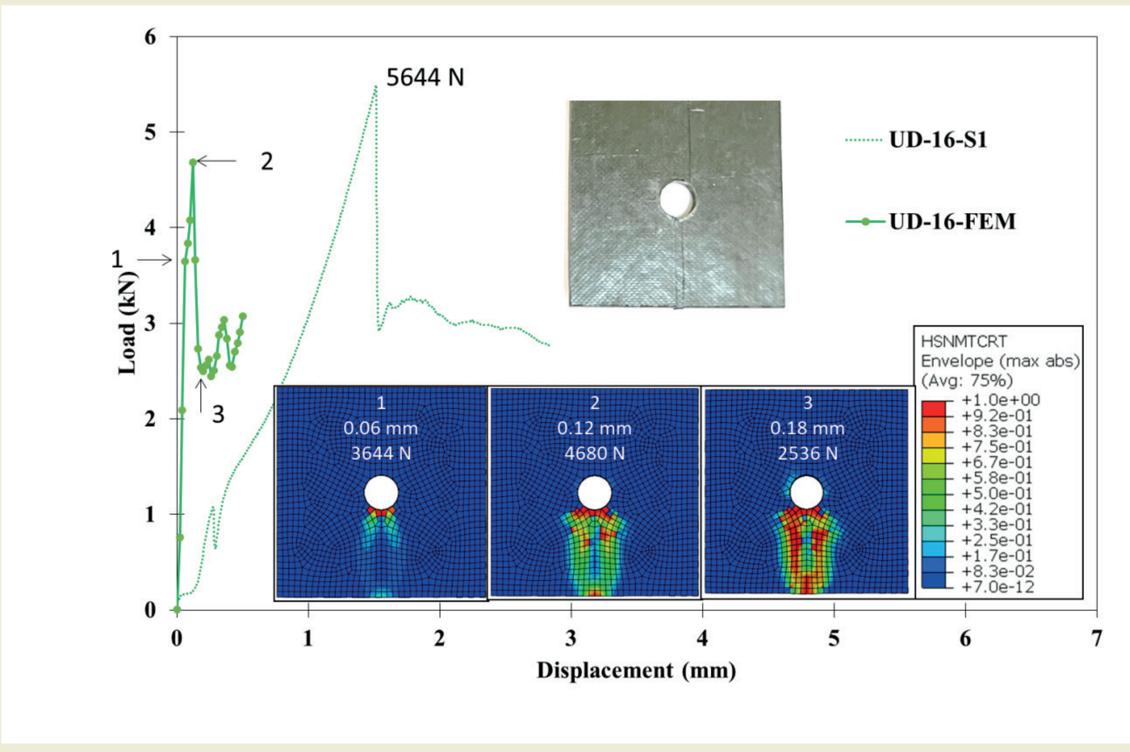

Figure 11. FEM prediction for UD-16 sample: load-displacement curve under the double-shear tensile test.

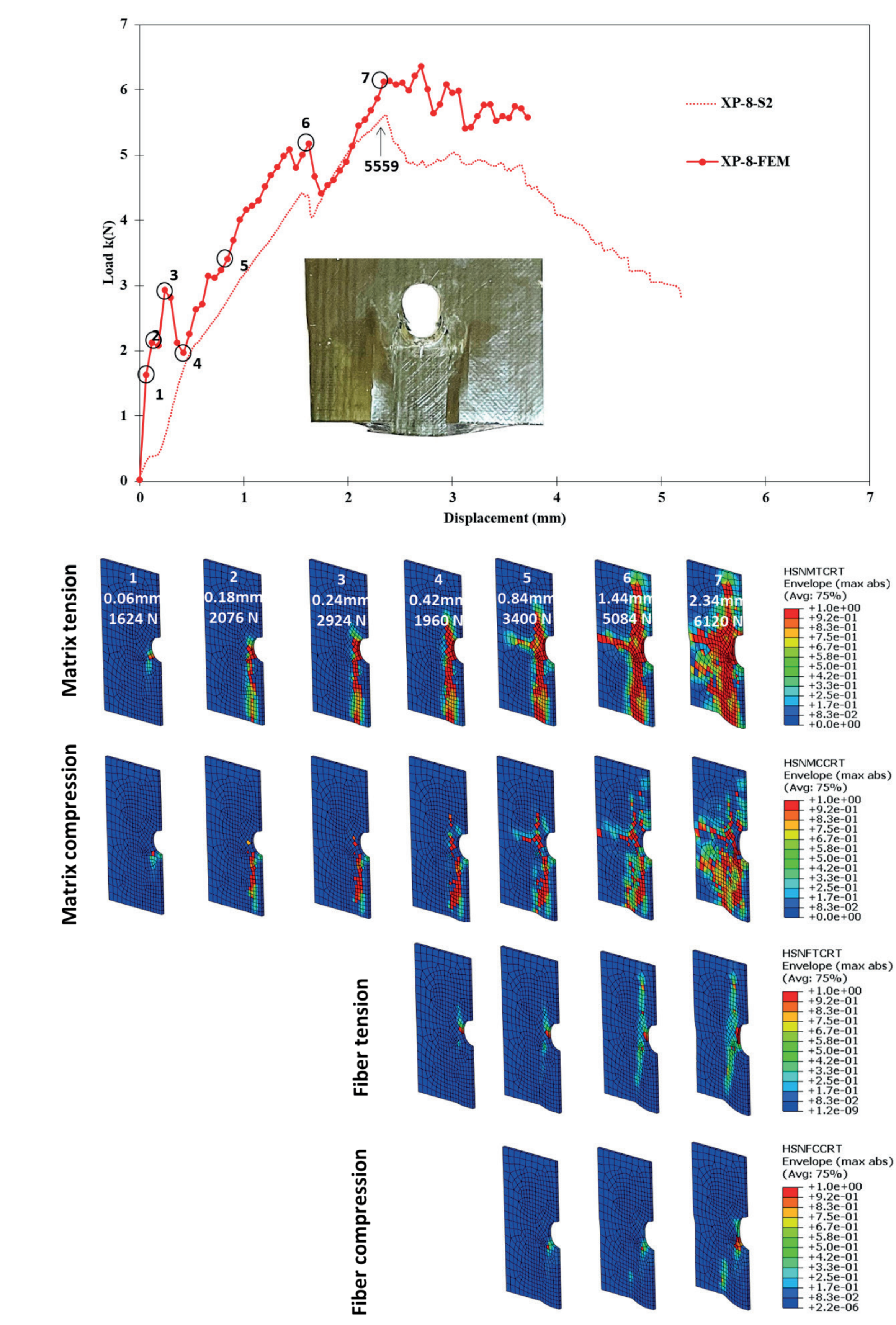

Figure 12. Comparison of FEM predictions and experimental results for the XP-8 specimen: Load–displacement response under double-shear tensile testing

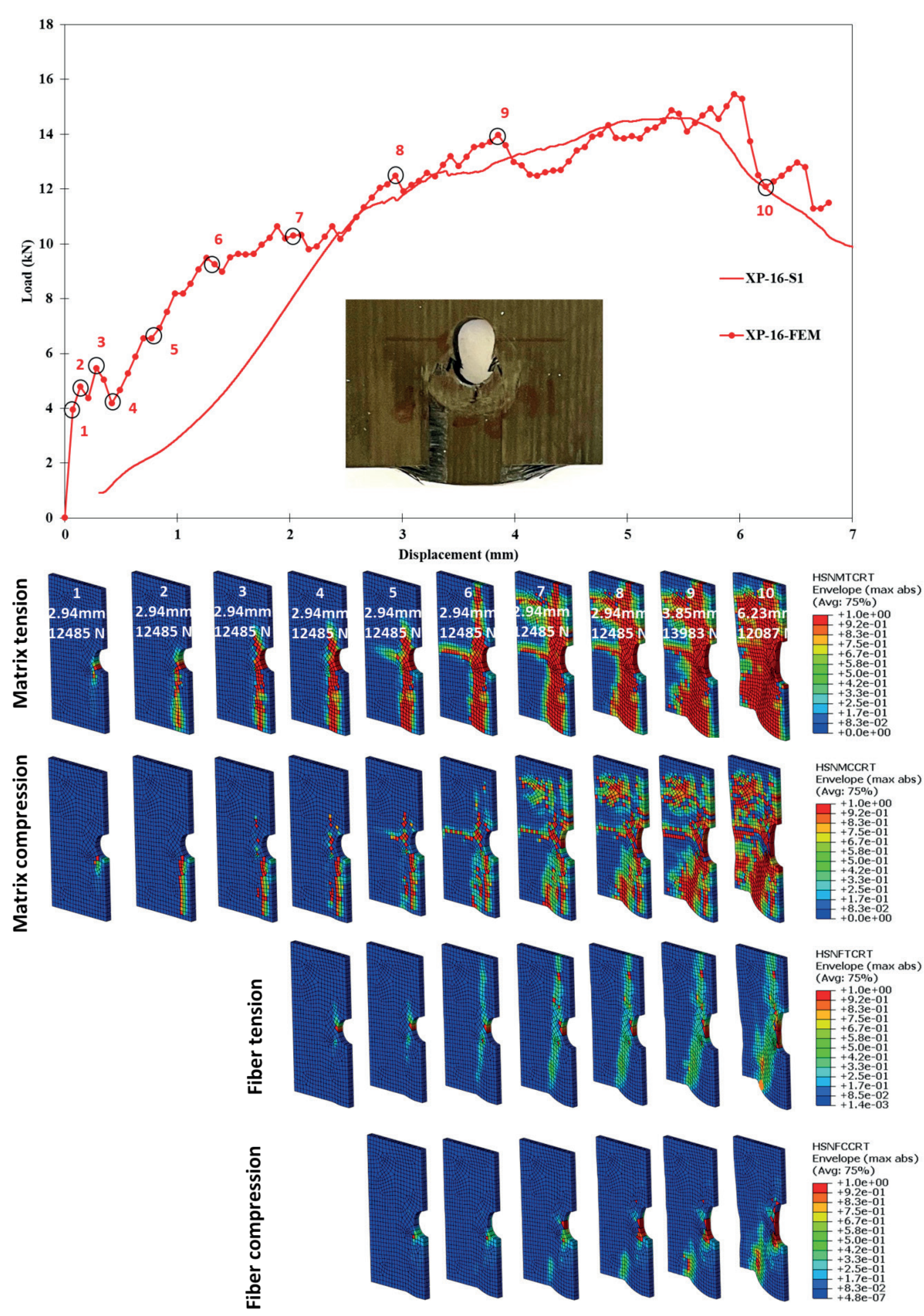

Figure 13. Comparison of FEM predictions and experimental results for the XP-16 specimen: Load–displacement response under double-shear tensile testing

13). As a result, each row in ▶Figure 12 includes seven frames, while ▶Figure 13 contains ten. This segmentation strategy reflects the specimen-specific damage progression representative visualization of failure development at significant mechanical events.

The load-displacement graph presents the pin-crush test results for cross-ply (XP) and unidirectional (UD) laminates with 16 plies, comparing experimental (EXP) and finite element (FEM) data, as shown in ▶Figure 14. Both XP and UD laminates exhibit an initial load increase followed by a peak and subsequent drop, characteristic of composite failure. The XP-16 laminates show higher peak loads than UD-16 laminates in both experimental and FEM results, indicating superior load-carrying capacity due to the cross-ply layup. While the FEM predictions generally follow experimental trends, some deviations are observed. The XP-16-FEM and UD-16-FEM overestimates the peak load compared to test one. In the modelling section, it was noted that delamination was not considered in the model due to computational burden. The higher values of FEM predictions may be come from this phenomenon. Additionally, the XP-16 laminates exhibit a more gradual load drop after peak, while the UD-16 laminates experience more abrupt failure, especially in experimental results.

4. Conclusions

This study investigated the bearing and pin-crush behaviors of cross-ply (XP) and unidirectional (UD) composite laminates through both experimental testing and finite element analysis (FEM). The results highlight the significant influence of laminate architecture on the mechanical response and failure mechanisms under these loading conditions. In bearing tests, XP laminates (XP-8 and XP-16) demonstrated superior load-carrying capacity compared to UD-16 laminates, attributed to the enhanced load redistribution and resistance to through-thickness shear provided by the cross-ply layup. The UD-16 laminates exhibited brittle failure, characterized by abrupt load drops and transverse matrix cracking, reflecting their inherent susceptibility to crack propagation along the fiber direction. The FEM simulations effectively captured the general trends of the experimental data, validating the models' ability to predict the bearing response and failure initiation. However, discrepancies in the post-peak regions suggest the need for further refinement in material modeling, particularly concerning damage propagation and softening behavior. Pin-crush tests further emphasized the performance advantages of XP-16 laminates, which exhibited higher peak loads and a more gradual post-peak load decline compared to UD-16 laminates. The XP-16 laminates demonstrated a progressive failure mechanism, while the UD-16 laminates experienced brittle failure with rapid damage accumulation. Digital Image Correlation (DIC) analysis revealed distinct strain distributions and failure modes for each laminate type, with XP-16 showing progressive strain accumulation and shear-out failure, and UD-16 displaying localized compressive strain and brittle crack propagation. FEM simulations of the pin-crush tests showed good qualitative agreement with experimental results, but quantitative discrepancies, especially in peak load predictions and post-peak behavior, indicate the need for improved material modeling.

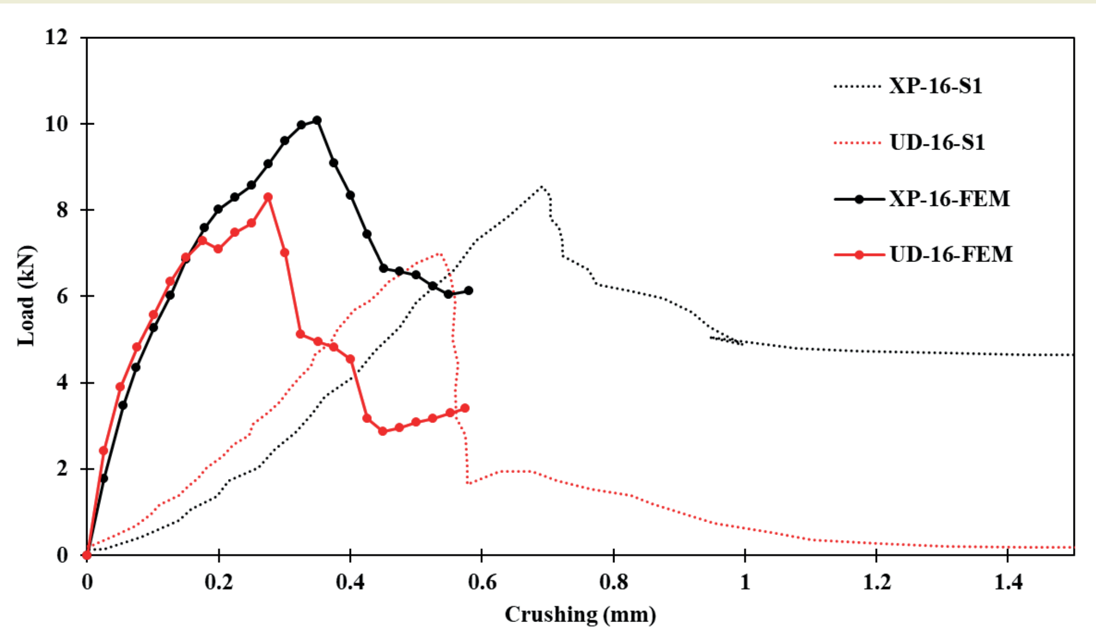

Figure 14. FEM prediction for UD-16 and XP-16 sample: load-displacement curve under the pin-crush test.

 https://doi.org/10.26701/ems.1643484

Acknowledgement

The author acknowledges the support of the Tekirdağ Namık Kemal University Research Fund under project code of NKUBAP.06.GAYP.24.549. Also, the author would like to express their sincere gratitude to the Boğaziçi University - Composites Laboratory for providing the necessary facilities, technical support, and equipment used throughout this research

Research ethics

Not applicable.

Author contributions

The author solely conducted all stages of this research.

Competing interests

The author states no conflict of interest.

Research funding

None declared.

Data availability

The raw data can be obtained on request from the corresponding author.

Peer-review

Externally peer-reviewed.

Orcid

Kenan Cinar https://orcid.org/0000-0001-7402-2032

References

[1] Furtado, C., Tavares, R. P., Arteiro, A., Xavier, J., Linde, P., Wardle, B. L., & Camanho, P. P. (2021). Effects of ply thickness and architecture on the strength of composite sub-structures. Composite Structures, 256, 113061. https://doi.org/10.1016/j.compstruct.2020.113061

[2] Okutan, B., & Karakuzu, R. (2003). The strength of pinned joints in laminated composites. Composites Science and Technology, 63(6), 893-905. https://doi.org/10.1016/S0266-3538(02)00313-5

[3] Cameron, C. J., Larsson, J., Loukil, M. S., Murtagh, T., & Wennhage, P. (2021). Bearing strength performance of mixed thin/thick-ply, quasi-isotropic composite laminates. Composite Structures, 261, 113312. https://doi.org/10.1016/j.compstruct.2020.113312

[4] [Okutan Baba] Okutan Baba, B. (2006). Behavior of pin-loaded laminated composites. Experimental Mechanics, 46, 589-600. https://doi.org/10.1007/s11340-006-8735-z

[5] Sen, F., Pakdil, M., Sayman, O., & Benli, S. (2008). Experimental failure analysis of mechanically fastened joints with clearance in composite laminates under preload. Materials & Design, 29(6), 1159-1169. https://doi.org/10.1016/j.matdes.2007.05.009

[6] Lim, T. S., & Kim, B. C. (2006). Fatigue characteristics of the bolted joints for unidirectional composite laminates. Composite Structures, 72(1), 58-68. https://doi.org/10.1016/j.compstruct.2004.10.013

[7] Khashaba, U. A., Sebaey, T. A., & Alnefaie, K. A. (2013). Failure and reliability analysis of pinned-joints composite laminates: Effects of stacking sequences. Composites Part B: Engineering, 45(1), 1694-1703. https://doi.org/10.1016/j.compositesb.2012.09.066

[8] Ataş, A., & Soutis, C. (2013). Subcritical damage mechanisms of bolted joints in CFRP composite laminates. Composites Part B: Engineering, 54, 20-27. https://doi.org/10.1016/j.compositesb.2013.04.071

[9] Xiao, Y., & Ishikawa, T. (2005). Bearing strength and failure behavior of bolted composite joints (part I: Experimental investigation). Composites Science and Technology, 65(7-8), 1022-1031. https://doi.org/10.1016/j.compscitech.2005.02.011

[10] Broutelle, M., Lachaud, F., Barrièrre, L., Daidié, A., Chardonneau, A., & Bouillon, F. (2020). Bearing damage identification in oxide/oxide ceramic matrix composite with a new test design. Composite Structures, 236, 111902. https://doi.org/10.1016/j.compstruct.2020.111902

[11] Zhuang, F., Chen, P., Arteiro, A., & Camanho, P. P. (2019). Mesoscale modelling of damage in half-hole pin bearing composite laminate specimens. Composite Structures, 214, 191-213. https://doi.org/10.1016/j.compstruct.2019.01.06

[12] Sola, C., Castanié, B., Michel, L., Lachaud, F., Delabie, A., & Mermoz, E. (2016). On the role of kinking in the bearing failure of composite laminates. Composite Structures, 141, 184-193. https://doi.org/10.1016/j.compstruct.2016.01.058

[13] Ireman, T. (1998). Three-dimensional stress analysis of bolted single-lap composite joints. Composite Structures, 43(3), 195-216. https://doi.org/10.1016/S0263-8223(98)00103-2

[14] McCarthy, M., McCarthy, C. T., Lawlor, V. P., & Stanley, W. F. (2005). Three-dimensional finite element analysis of single-bolt, single-lap composite bolted joints: part I—model development and validation. Composite Structures, 71(2), 140-158. https://doi.org/10.1016/j.compstruct.2004.09.024

[15] Tserpes, K. I., Papanikos, P., & Kermanidis, T. H. (2001). A three-dimensional progressive damage model for bolted joints in composite laminates subjected to tensile loading. Fatigue & Fracture of Engineering Materials & Structures, 24(10), 663-675. https://doi.org/10.1046/j.1460-2695.2001.00424.x

[16] Montagne, B., Lachaud, F., Paroissien, E., Martini, D., & Congourdeau, F. (2020). Failure analysis of single lap composite laminate bolted joints: Comparison of experimental and numerical tests. Composite Structures, 238, 111949. https://doi.org/10.1016/j.compstruct.2020.111949

[17] Hu, X. F., Haris, A., Ridha, M., Tan, V. B. C., & Tay, T. E. (2018). Progressive failure of bolted single-lap joints of woven fibre-reinforced composites. Composite Structures, 189, 443-454. https://doi.org/10.1016/j.compstruct.2018.01.104

[18] Wang, J., Qin, T., Mekala, N. R., Li, Y., Heidari-Rarani, M., & Schröder, K. U. (2022). Three-dimensional progressive damage and failure analysis of double-lap composite bolted joints under quasi-static tensile loading. Composite Structures, 285, 115227. https://doi.org/10.1016/j.compstruct.2022.115227

[19] Nerilli, F., & Vairo, G. (2017). Progressive damage in composite bolted joints via a computational micromechanical approach. Composites Part B: Engineering, 111, 357-371. https://doi.org/10.1016/j.compositesb.2016.11.056

[20] Qingyuan, L., Zhao, Y., Yan, C., Liu, Y., & Pan, W. (2024). Progressive bearing failure analysis and strength prediction method for the initial assembly and tensile process of composite bolted joints. Composites Part A: Applied Science and Manufacturing, 187, 108476. https://doi.org/10.1016/j.compositesa.2024.108476

[21] Joseph, A. P., Davidson, P., & Waas, A. M. (2018). Progressive dama-

ge and failure analysis of single lap shear and double lap shear bolted joints. Composites Part A: Applied Science and Manufacturing, 113, 264-274. https://doi.org/10.1016/j.compositesa.2018.07.01

[22] Shipsha, A., & Burman, M. (2020). Failure mechanisms in NCF composite bolted joints: Experiments and FE model. Composites Part B: Engineering, 192, 107950. https://doi.org/10.1016/j.compositesb.2020.107950

[23] Cinar, K. (2024). Enhancement of laminate open-hole tensile strength by considering fiber waviness around holes. Journal of Manufacturing Processes, 131, 766-780. https://doi.org/10.1016/j.jmapro.2024.09.079

[24] Li, A., Zhang, H., & Yang, D. (2025). Bearing performance and progressive failure analysis of bolted joint in 3D printed pseudo-woven CFRP composite with fibre steering. Composites Part A: Applied Science and Manufacturing, 188, 108526. https://doi.org/10.1016/j.compositesa.2024.108526

[25] Abaqus Analysis User's. Manual. Online Documentation Help: Dassault Systemes; 2016

[26] Falcó, O., Ávila, R.L., Tijs, B., & Lopes C.S. (2018). Modelling and simulation methodology for unidirectional composite laminates in a Virtual Test Lab framework, Composite Structures, 190, 137-159. https://doi.org/10.1016/j.compstruct.2018.02.016